SEMARAK ILMU PUBLISHING

Journal of Advanced Research in Fluid Mechanics and Thermal Sciences

Journal homepage:
https://semarakilmu.com.my/journals/index.php/fluid_mechanics_thermal_sciences/index
ISSN: 2289-7879

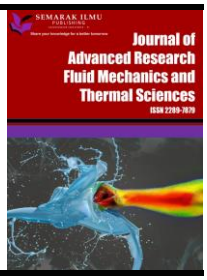

Investigating Dual Inlet Cyclone Separator Performance: Effects of Vortex Finder Diameter, Shape, and Particle Diameter on Separation Efficiency and Pressure Drop

Saikat Barua[1,*], Mohd Faizal Mohideen Batcha[2], Azriszul Mohd Amin[1], Akmal Nizam Mohammed[1], Makatar Wae-hayee[3]

[1] Faculty of Mechanical and Manufacturing Engineering, Universiti Tun Hussein Onn Malaysia, 86400 Parit Raja, Johor, Malaysia
[2] Center for Energy and Industrial Environment Studies (CEIES), Faculty of Mechanical and Manufacturing Engineering, Universiti Tun Hussein Onn Malaysia, 86400 Parit Raja, Johor, Malaysia
[3] Energy Technology Research Center, Faculty of Engineering, Prince of Songkla University, Hatyai, Songkhla 90110, Thailand

ARTICLE INFO

Article history:
Received 31 May 2024
Received in revised form 28 August 2024
Accepted 10 September 2024
Available online 30 September 2024

Keywords:
Cylone separator; bortex finder; CFD; K-ε RNG

ABSTRACT

The diameter and shape of the vortex finder of cyclone separator plays a significant role in separation efficiency and pressure drop. Currently, there have been many studies conducted on the shape and ratio of vortex finder of cyclone separator. This paper aims to compare numerical results of Raynold stress turbulence model RSM with K-ε RNG numerical analysis results and analyse the effect of further variation of the vortex finder diameter and shape of dual inlet cyclone separators. Five variation of vortex finder diameters namely 291mm, 310mm, 330mm, 348mm, and 366mm, four types of vortex finder shapes namely normal (cylindrical), spiral, divergent and spiral-divergent have been studied with different particle diameter and constant inlet velocity. The result obtained from this study suggests that increasing the vortex finder diameter have negative effect on separation efficiency. It also shows that increasing the vortex finder diameter consistently decrease the pressure drop. From the result, it is been found that the 291mm vortex finder has higher separation efficiency than the rest. Analysis with different vortex shapes, the spiral-divergent shape proved to be best in terms of separation efficiency.

1. Introduction

Cyclones are tools for separating two phases of a fluid flow in this context. These are the well-known inverted cones seen in dust-extraction systems, without which many a carpenter's shop or wheat mill would be destroyed by a dust agglomeration [1]. Dust-filled air or gas is introduced tangentially at one or more places and exits via the centre of a cylindrical or conical chamber. Due to their inertia, the dust particles prefer to travel in a direction that leads them into a receiver outside

* *Corresponding author.*
E-mail address: saikatuthm@gmail.com

https://doi.org/10.37934/arfmts.121.2.90105

the separator wall [2]. The cyclone separator has been utilized in industrial settings for a very long time, including power generation, gas turbines, chemical reactions, and others [3].

Li *et al.,* [4] conducted research on the impact of the wedge-shaped roof geometry on the functionality of the cyclone separator. A specific configuration with a height of 0.29831 m and a top diameter of 0.17582 m, resulting in a 4.2% increase in collection efficiency and an 11% increase in pressure drop compared to the initial state, shows significant improvements for multi-objective optimization, which reveals nonlinear relationships between collection efficiency and pressure drop.

At an input velocity of U_{in} = 12 m/s, Brar and Wasilewski [5] analyse the effects of increasing temperature on the pressure drop and collecting efficiency. According to the results, pressure drop decreased with increasing gas temperature, but collection efficiency declined and cut-off particle size rose. Overall, especially in high-temperature settings, the innovative cyclone designs outperformed the conventional model, providing up to 60% greater separation efficiency.

Panday and Brar [6] provide a proposal and examine the effectiveness of unique cyclone separators with bulged conical sections in a different investigation. Results revealed that when compared to the Std model, the proposed models had somewhat lower collection efficiency (up to 33% decrease) but reduced pressure losses (up to 28% reduction). Due to their greater separation distance and substantially lower pressure drop, these curved conical shapes work best as pre-separators.

In a study by Bumrungthaichaichan [7], mean flow patterns and performance are taken into account while evaluating numerical techniques for CFD simulations of cyclone separators. The QNS-based model proved to be more accurate in predicting pressure drops, whereas the MNS-based model provided quicker simulations. Two numerical scheme sets, QNS and MNS, were compared.

Fatahian *et al.,* [8] suggested a numerical methodology based on a three-dimensional CFD analysis and the Taguchi approach to evaluate the performance of the square cyclone and identify the ideal operating conditions that would provide the system's best separation efficiency. Investigated variables were intake temperature, inlet velocity, particle mass flow rate, and turbulence intensity; inlet velocity turned out to be the most significant one. 20 m/s intake velocity, 300 K inlet temperature, 180 g/min mass flow rate, and 4% turbulence intensity were found to be the best parameters for the maximum separation efficiency, which resulted in a 76% separation efficiency for 16 m particles.

Sardar *et al.,* [9] use tests and computer simulations to study the performance of two linked cyclones, 2D2D and 1D3D. The pressure loss in both cyclones is found to be considerably increased by increasing intake velocity, although adding a second cyclone in series helps minimize pressure drop, especially for tiny particles.

Using numerical simulations, Chaghakaboodi and Saidi [10] investigated the effect of vortex finder shape on square cyclone separator performance. Different hydraulic diameter vortex finders were taken into consideration. The findings demonstrated that decreasing the hydraulic diameter of the vortex finder boosted pressure drop and separation efficiency, particularly with a notable rise in pressure drop when the diameter was reduced from 0.5 to 0.25.

Yand *et al.,* [11] propose adding helical triangular fins to the inner cylinder wall to improve cyclone separator performance. The ideal fin parameters were chosen using numerical simulations and optimization methods. The results showed that, despite a modest increase in pressure drop caused by the fins, collection efficiency was greatly enhanced due to a decrease in the cut-off diameter and turbulent kinetic energy.

A multi-objective genetic algorithm (MOGA) and CFD simulation are used by Gopalakrishnan *et al.,* [12] to optimize the design of an axial swirl tube cyclone separator. A second-order regression model was created using Taguchi and ANOVA analysis after four crucial factors (the number of blades,

the blade length, the blade angle, and the distance from the blade output tube) were determined. In comparison to the reference model, MOGA produced a set of 18 Pareto fronts with the best performance in terms of pressure drop and filtering effectiveness.

A cylinder vortex stabilizer is inserted in the cyclone body's centre in Guo *et al.,* [13], which focuses on a revolutionary improvement to cyclone separators. It improves stability, mitigates whirling frequency, and dramatically lowers tangential velocity, leading to greater separation efficiency and less turbulence, which can lessen vibration and noise.

Yao *et al.,* [14] looked at how a gas-solid cyclone separator's performance and flow patterns are impacted by the spatial distribution of intake particles. The effectiveness of separation was increased by decreasing the intake particle flow area and placing particles lower. The dispersed particles and back-mixing within the cyclone were primarily affected by the vertical particle distribution, which had a greater effect than the horizontal distribution.

Wang *et al.,* [15] studied dual inlet cyclones with 330mm vortex diameter. In this study, a dual inlet cyclone separator was studied for its potential use in biomass processing facilities, as reported by our previous studies [16,17]. Dual inlet cyclones can be effective in large biomass processing plants with multiple processing equipment such as drum dryers and shredders as a mean to reduce initial as well as maintenance costs. Therefore, in our previous work Barua *et al.,* [18], this paper reports the numerical study using the turbulence model K- ε RNG to observe the effect of separation efficiency and pressure drop with the variation of vortex inlet diameter and shape. The work by Wang *et al.,* [11] was used for validation purposes of the present study.

2. Methodology

2.1 Computational Geometry

Figure 1, depicts the cyclone separator's geometry model and meshing model. The cyclone separator's geometric structure is specified by several geometry parameters, and Table 1 displays its dimensions. Figure 2, Shows the cross-sectional view of different vortex finder shapes. From left to right the shapes are names as Normal, Spiral, Divergent and Spiral Divergent.

Table 1
Dimensions of impacting parameters

Geometry	Dimension
Barrel diameter, D/mm	900
Vortex finder diameter, De/mm	291/310/330/348/ 366
Vortex finder length, S/mm	419
Vortex finder length (Outer), mm	300
Inlet height, a/mm	419
Inlet weidth, b/mm	176
Inlet length, mm	500
Barrel height, h/mm	1638
Cone height, He/mm	1620
Cone bottom diameter, Dc/mm	360
Bin diameter, Be/mm	630
Dipleg diameter, Dd/mm	156
Dipleg length, Hd/mm	800
h1/mm, h2/mm, h3/mm	250.750,700

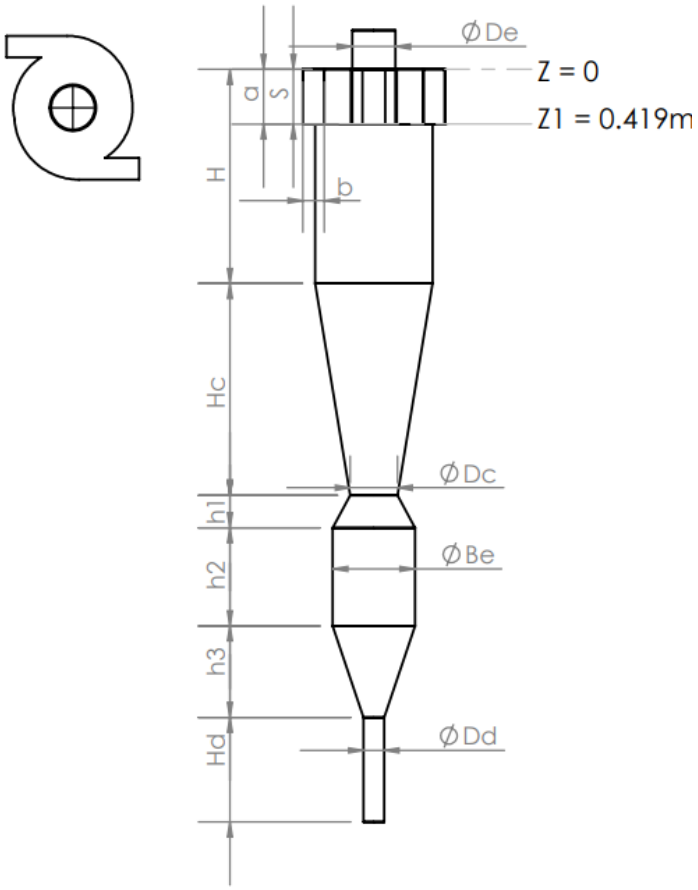

Fig. 1. Geometry with dimension of impacting parameters

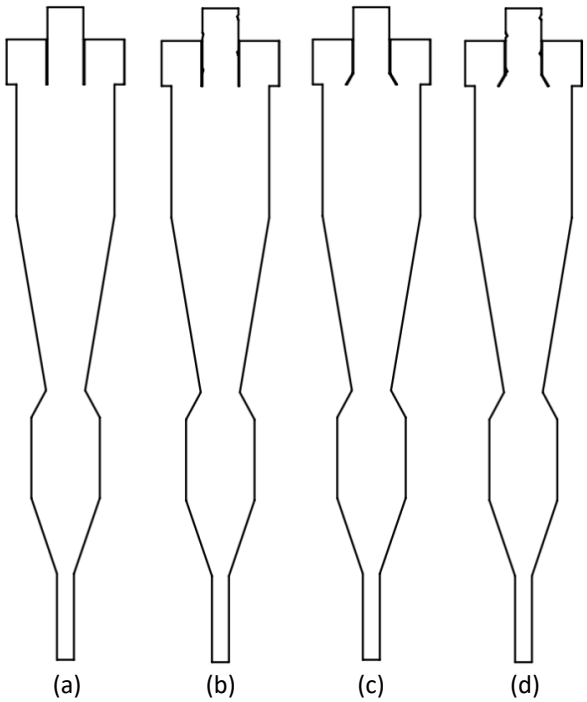

Fig. 2. Cross sectional view of different vortex finder shape cyclone separator (a)Traditional (normal), (b) Spiral (c) Divergent, and (d) Spiral divergent

2.2 Governing Equation

The simulation tackles incompressible fluid flow within Ansys-Fluent. The Navier-Stokes equations consist of three equations for the conservation of mass, momentum, and energy. In this study, considering an incompressible flow therefore density ρ is constant. The governing equation for the fluid flow is the following form of the incompressible continuity equations for the fluid flow and also the Navier-Stokes momentum equations.

The continuity equation given in the very first equation can be expressed in cylindrical coordinates as [19]:

$$\frac{\partial \rho}{\partial t}+\frac{1}{r}\frac{\partial(\rho r V_r)}{\partial r}+\frac{1}{r}\frac{\partial(\rho V_\theta)}{\partial \theta}+\frac{\partial(\rho V_z)}{\partial z}=0 \tag{1}$$

The Navier-Stokes equations given in the first equation can be expressed in cylindrical coordinates as (r, θ, z):

r Momentum:

$$\rho\left(\frac{v_\theta}{\partial t}+v_r\frac{\partial v_r}{\partial r}+\frac{\partial v_r}{\partial \theta}+v_z\frac{v_\theta^2}{\partial z}-\frac{\partial p}{r}\right)=-\frac{\partial}{\partial r}+\mu\left[\frac{\partial}{\partial r}\left(\frac{1}{r}\frac{\partial}{\partial r}(rv_r)\right)+\frac{1}{r^2}\frac{\partial^2 v_r}{\partial \theta^2}+\frac{\partial^2 v_r}{\partial z^2}-\frac{2}{r^2}\frac{\partial v_\theta}{\partial \theta}\right]+\rho g_r \tag{2}$$

θ Momentum:

$$\left(\frac{\partial v_\theta}{\partial t}+v_r\frac{\partial v_\theta}{\partial r}+\frac{v_\theta}{r}\frac{\partial v_\theta}{\partial \theta}+v_z\frac{\partial v_\theta}{\partial z}+\frac{v_r v_0}{r}\right)=$$
$$-\frac{1}{r}\frac{\partial p}{\partial \theta}+\mu\left[\frac{\partial}{\partial r}\left(\frac{1}{r}\frac{\partial}{\partial r}(rv_\theta)\right)+\frac{1}{r^2}\frac{\partial^2 v_\theta}{\partial \theta^2}+\frac{\partial^2 v_\theta}{\partial z^2}+\frac{2}{r^2}\frac{\partial v_r}{\partial \theta}\right]+\rho g_\theta \tag{3}$$

z Momentum:

$$\rho\left(\frac{\partial v_z}{\partial t}+v_r\frac{\partial v_z}{\partial r}+\frac{v_\theta}{r}\frac{\partial v_z}{\partial \theta}+v_z\frac{\partial v_z}{\partial z}\right)=-\frac{\partial p}{\partial z}+\mu\left[\frac{1}{r}\frac{\partial}{\partial r}\left(r\frac{\partial v_z}{\partial r}\right)+\frac{1}{r^2}\frac{\partial^2 v_z}{\partial \theta^2}+\frac{\partial^2 v_z}{\partial z^2}\right]+\rho g_z \tag{4}$$

The k-epsilon turbulence model is based on two transport equations, one for turbulent kinetic energy (k) and the other for the turbulent dissipation rate (epsilon) [20].

Transport Equation for k:

$$\frac{\partial}{\partial t}(\rho k)+\frac{\partial}{\partial x_i}(\rho k u_i)=\frac{\partial}{\partial x_j}\left[\left(\mu+\frac{\mu_t}{\sigma_k}\right)\frac{\partial k}{\partial x_j}\right]+P_k-\rho\varepsilon \tag{5}$$

where,
ρ is the fluid density,
ui is the velocity component in the *i* direction,
μ is the molecular viscosity,
μt is the turbulent viscosity,
σk is the Prandtl number for turbulent kinetic energy,
Pk represents the production of turbulent kinetic energy,
ε is the turbulent dissipation rate.

Transport Equation for epsilon:

$$\frac{\partial}{\partial t}(\rho\varepsilon) + \frac{\partial}{\partial x_i}(\rho\varepsilon u_i) = \frac{\partial}{\partial x_j}\left[\left(\mu + \frac{\mu_t}{\sigma_\varepsilon}\right)\frac{\partial \varepsilon}{\partial x_j}\right] + C_{\varepsilon 1}\frac{\varepsilon}{k}P_k - C_{\varepsilon 2}\rho\frac{\varepsilon^2}{k} \quad (6)$$

The RNG model introduces additional terms into the transport equations for *k* and *ε* to improve accuracy. These additional terms are derived using concepts from renormalization group theory.

RNG Modified Transport Equations:

$$\frac{\partial}{\partial t}(\rho k) + \frac{\partial}{\partial x_i}(\rho k u_i) = \frac{\partial}{\partial x_j}\left[\left(\mu + \frac{\mu_t}{\sigma_k}\right)\frac{\partial k}{\partial x_j}\right] + P_k - \rho\varepsilon + \frac{\partial}{\partial x_j}\left[(\mu_t\sigma_k)\frac{\partial \beta}{\partial x_j}\right] \quad (7)$$

$$\frac{\partial}{\partial t}(\rho\varepsilon) + \frac{\partial}{\partial x_i}(\rho\varepsilon u_i) = \frac{\partial}{\partial x_j}\left[\left(\mu + \frac{\mu_t}{\sigma_\varepsilon}\right)\frac{\partial \varepsilon}{\partial x_j}\right] + C_{\varepsilon 1}\frac{\varepsilon}{k}P_k - C_{\varepsilon 2}\rho\frac{\varepsilon^2}{k} + \frac{\partial}{\partial x_j}\left[(\mu_t\sigma_\varepsilon)\frac{\partial \beta}{\partial x_j}\right] \quad (8)$$

Where:

β is the additional variable introduced by the RNG model,

The terms involving β are responsible for improving the model's performance, particularly in adverse pressure gradient flows.

The constants σk, $\sigma\varepsilon$, $C_{\varepsilon 1}$, $C_{\varepsilon 2}\rho$, and other model coefficients are typically calibrated based on experimental or DNS (Direct Numerical Simulation) data for different flow conditions.

2.3 Boundary Conditions

In the simulation setup, gas enters the cyclone separator through the intake pipe, and a velocity-inlet condition is imposed at this inlet boundary. The hydraulic dimeter of the inlet is set to 0.2476 m and the pressure outlet hydraulic dimeter is 0.330 m. The turbulence intensity is set to 3.5% and 3.36% for inlet and outlet. The Vortex finder pressure-outlet boundary condition is set to 0 Pa as open to atmospheric pressure.

To evaluate the effect and performance of particle collection efficiency and pressure drop three types of vortex finder is analyzed, which has diameters of 291mm, 310mm, 330mm, 348mm and 366mm. Particle density 2700 kg/m^3 for validation and 1750 kg/m^3 for performance analysis. The particle sizes are 1, 5, 7, 10, and 12 µm in the simulations. Inlet velocity 15.5 m/s used for validation and 12 m/s constant velocity used for this current analysis.

The diagram in Figure 3, shows the surfaces defined as Inlet, Pressure Outlet, and Particle Trap surface in the geometry. Micro particles enter the cyclone separator through the inlets and these surfaces are defined as reflect surface in the DPM (Discrete phase model). The Particle trap, which is configured as a trap border, serves as the particle discharge point for the cyclone separator. Pressure Outlet is characterized as escape route for clean gas that also captures the particles when particles manage to escape through the exhaust pipe. The other surfaces are defined as walls as they are intended to reflect as an entirely elastic collision. On these wall boundaries, the normal wall function and a no-slip condition are used to make sure that the gas and particles stick to the wall out of friction.

The COUPLE solver is used to simulate the pressure-velocity field interaction in the K-ε RNG turbulence model. To increase accuracy, the gradient computation is based on a least squares cell-

centered strategy. For accurate calculation of the pressure field, turbulent kinetic energy, momentum a second-order pressure technique is employed. The second-order upwind approach is also used to calculate the particular dissipation rate. The combination of these numerical approaches helps to accurately represent the fluid turbulence and flow patterns inside the cyclone separator.

2.4 Grid Independency Test

The grid independence test was run with five different grid numbers: 176018, 240098, 342952, 440281 and 528379 each with a different element number, pressure drop, y-velocity value and collection efficiency (Table 2). The Y velocity difference is about 5.7% between the 176018 and 342952 elements, however the difference drops to 0.2% between 440281 to 528379. The pressure drop difference between the 176018 and 342952 elements was consequently around 12%, where for 440281 to 528379 it drops to 3%. These data led to the conclusion that the 440281 elements produced satisfactory results with little fluctuation in pressure drop and Y-velocity. In order to ensure accuracy and computational efficiency, the 27mm (440281 elements) grid size was chosen as the best option for the simulation. Figure 3 and Table 2 provided below illustrate the tetrahedral mesh and associated meshing data.

Table 2
Grid Independency Test

Element	Pressure Drop (Pa)	Y – Velocity (m/s)	Separation Efficiency (%)
176018	1038.15	23.28	97.15
240098	1101.71	23.04	97.34
342952	1162.35	24.60	94.78
440281	1210.44	24.92	92.95
528379	1246.69	24.96	93.03

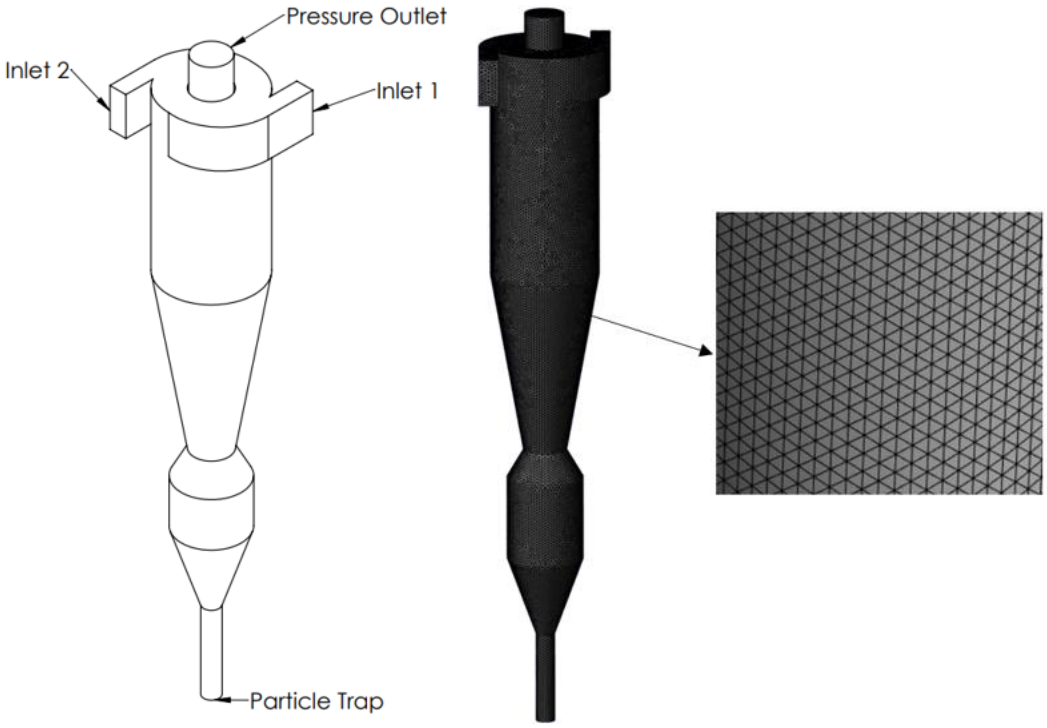

Fig. 3. Schematic diagram and geometry Meshing Model consisting of nearly 0.44 million elements

Tangential velocity and axial velocity are important quantities that define how the fluid travels in the context of fluid flow within cylindrical or circular geometries (Figure 4). A fluid's speed in a circular or tangential direction around the central axis is referred to as its tangential velocity. Axial velocity refers to the component of velocity along the longitudinal axis of a fluid flow. In other words, it is the velocity of fluid particles in the direction of flow. For example, in a cylindrical pipe, the axial velocity represents how fast the fluid is moving parallel to the pipe's length.

For the tangential velocity, the measurements are taken at radial positions ranging from -0.45 to 0.45, where 0 represents the centre of the cyclone. Typically, tangential velocity is highest near the walls due to the centrifugal force and decreases towards the centre in a cyclone separator. This is because the rotational motion is more pronounced at the periphery to aid in the separation process. The data reflects this trend as with higher velocities noted at positions further from the centre (Figure 4). The 440281 elements provide a high tangential velocity which is beneficial for particle separation. The profile shows less fluctuation and a more stable tangential velocity, which implies efficient separation with minimal re-entrainment. The difference in mesh size affects the velocity profiles, possibly due to changes in resistance and flow patterns within the separator.

Axial velocity in a cyclone separator is influenced by the centrifugal forces and the downward spiral motion of the particles. At the centre (0.0m radial position), the axial velocity reaches its minimum value for all diameters (Figure 4). As we move away from the centre towards the outer regions (both positive and negative radial positions) the axial velocity gradually increases. The overall trend remains consistent for all mesh sizes for all variations in actual values. The relatively smooth curves indicating stable flow behaviour. From the graph, it can be observed that there are minimal changes between 440281 to 528379 elements, however 528379 elements show disbalance on left side.

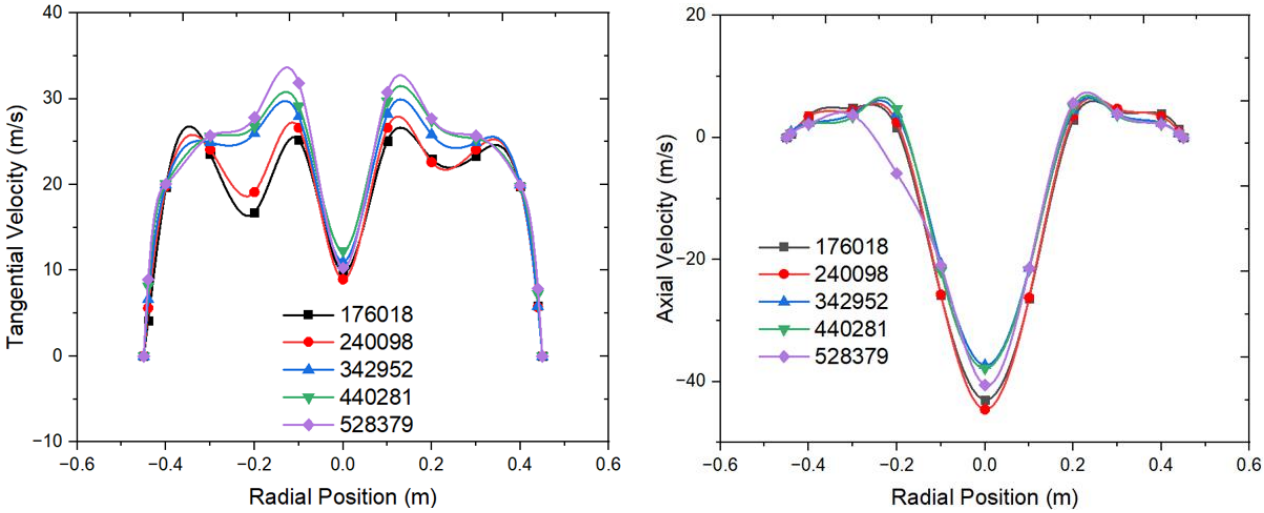

Fig. 4. Tangent and axial Velocity at Z = - 0.419m (Vortex finder bottom)

3. Results

Figure 5 compares the current numerical results with Wang *et al.,* [11]. In their study Wang *et al.,* [11] had used Raynold Stress turbulence model (RSM) and the current numerical used K-e RNG turbulence model. The average deviation between these two results is less than 2 % with higher deviation is 4.76 %.

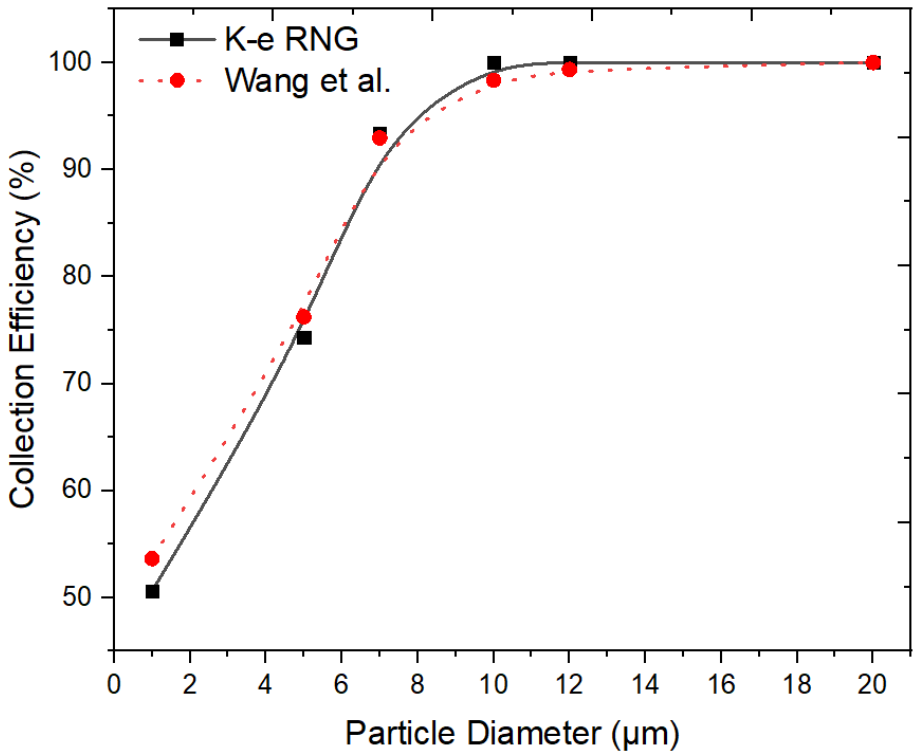

Fig. 5. Comparison of current result with literature

The flow trajectory within cyclone separators is crucial for effective particle separation, as depicted by five cyclone separators with varying vortex finder diameters. Figure 6(a) shows that the cyclone separator with the largest vortex finder diameter (366mm) exhibits the lowest particle separation efficiency, while the smallest diameter (291mm and 310mm) has a slightly higher efficiency. The average particle collection efficiency of 291mm vortex finder is 1.78% higher than 330mm and 2.24 % higher than 366mm vortex finder. This trend suggests that larger vortex finder diameters may facilitate less efficient particle-gas separation within the cyclone separator.

Figure 7(a) illustrates the relationship between Pressure Drop (pa) and Vortex Finder Diameter (mm) in cyclone separators. Each data point represents a specific vortex finder diameter: 291mm,310mm, 333mm, 348mm, and 366mm.The graph shows a negative linear correlation, as the vortex finder diameter increases, the pressure-drop decreases.

Figure 6(b) displays particle collection efficiency of four different vortex finder shapes Normal, Spiral, Divergent, and Spiral Divergent. Although, there is no significant difference observed between the shapes however, spiral divergent achieved distinguished particle collection efficiency for 1 and 7 μm diameter particles. In terms of pressure drop spiral divergent score high compare among other shapes while divergent shape results lowest pressure drop (Figure 7(b)). Having a lesser pressure drop means it requires less energy compared to other shapes.

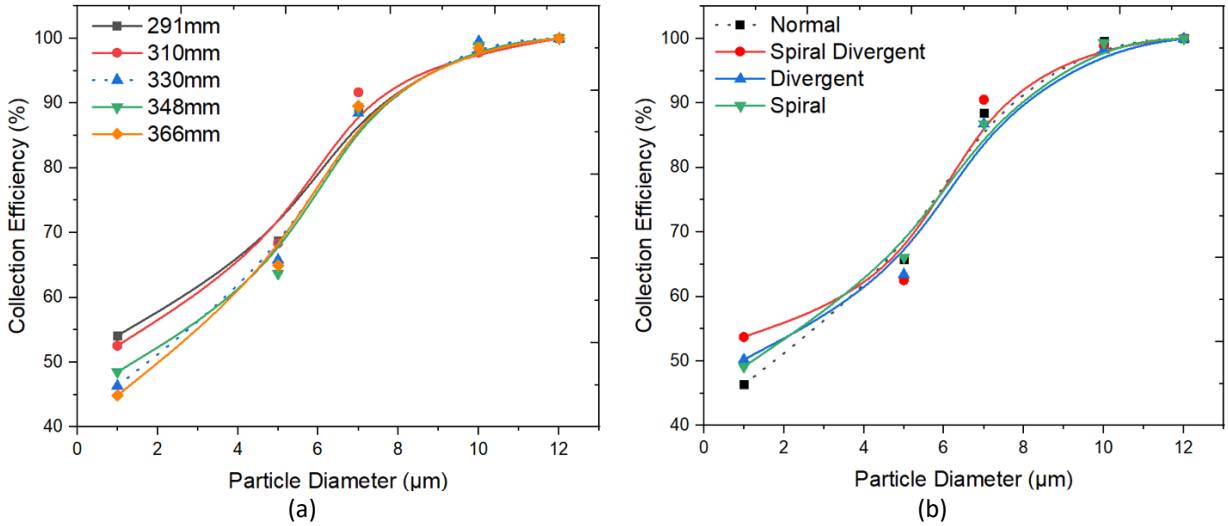

Fig. 6. Collection efficiency of different vortex finder diameter and shape

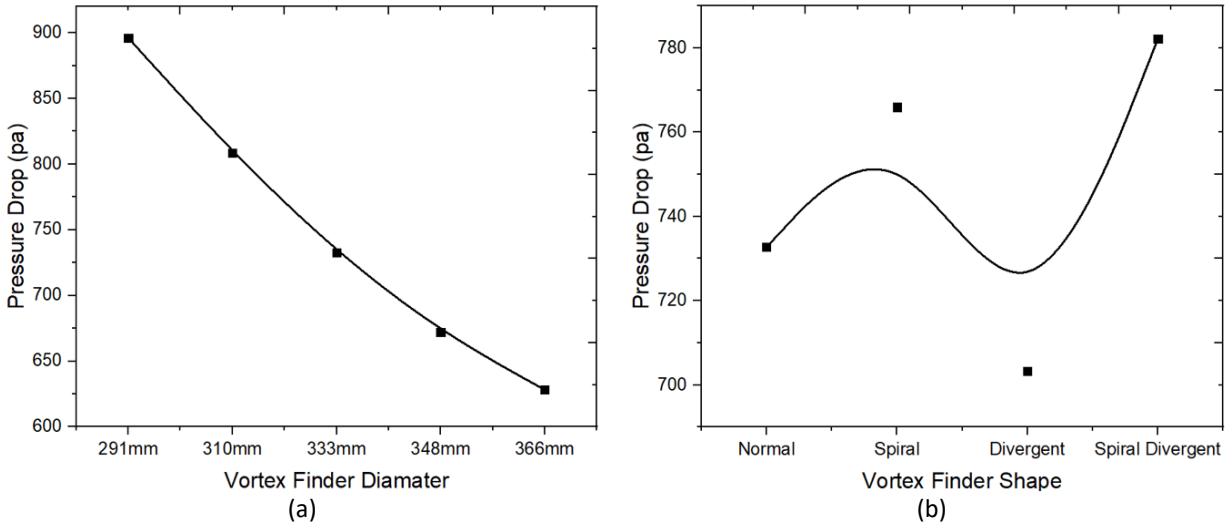

Fig. 7. Pressure drops of different vortex finder diameter and shape

The Spiral vortex finder presents (Figure 8(a)) higher tangential velocity at left side compared to the Normal shape. This increased velocity suggests stronger centrifugal forces, which enhances particle separation efficiency. Conversely, the Divergent vortex finder shows lower tangential velocities, which could reduce the centrifugal force and potentially decrease separation efficiency. The Spiral Divergent finder combines features of both Spiral and Divergent shapes, showing a moderate tangential velocity profile that balances the benefits of high rotational speeds.

In terms of axial velocity (Figure 8(b)), the Normal vortex finder displays a symmetrical profile with moderate depth indicating stable axial flow crucial for consistent particle separation. The Spiral vortex finder maintains symmetry but shows a slightly deeper axial velocity trough which can enhance particle settling but also increase the risk of re-entry. The Divergent vortex finder has a less deep axial velocity profile, promoting even axial flow that can reduce turbulence and support smoother particle separation. The Spiral Divergent vortex finder shows a well-balanced axial velocity profile, combining the benefits of increased tangential forces and stable axial flow, potentially offering the best overall performance.

It becomes evident that Spiral vortex finders significantly enhance particle separation through higher tangential velocities but at the cost of potentially higher pressure drops and increased

turbulence. Divergent vortex finders, on the other hand, promote stable flow with lower tangential velocities and reduce pressure drops. The Spiral Divergent vortex finder appears to offer a balanced solution to optimize both separation efficiency and operational stability by combining higher tangential velocities with stable axial flow.

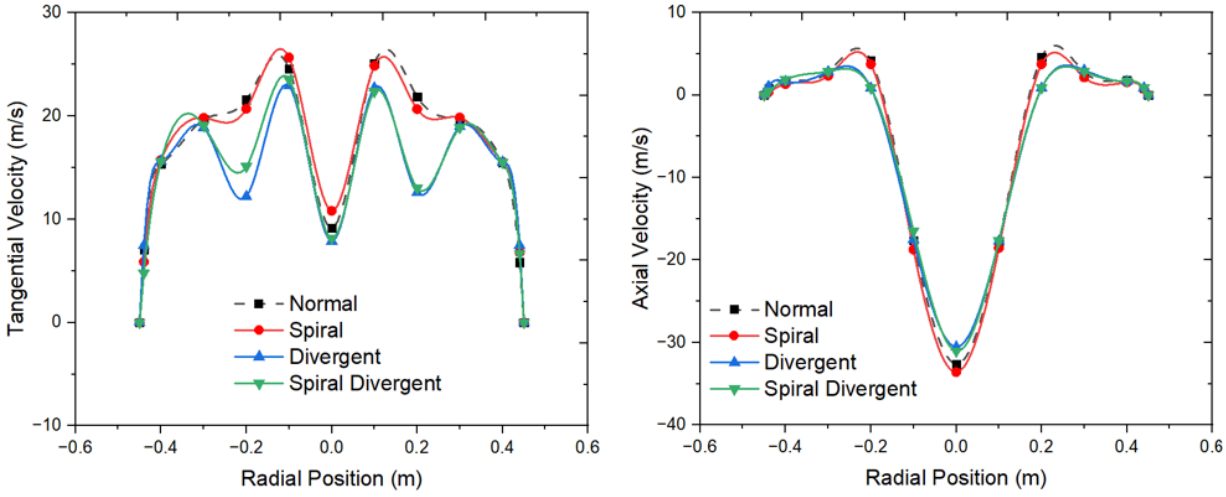

(a) (b)

Fig. 8. Tangential and axial velocity of different vortex finder shape at Z1 = 0.419m

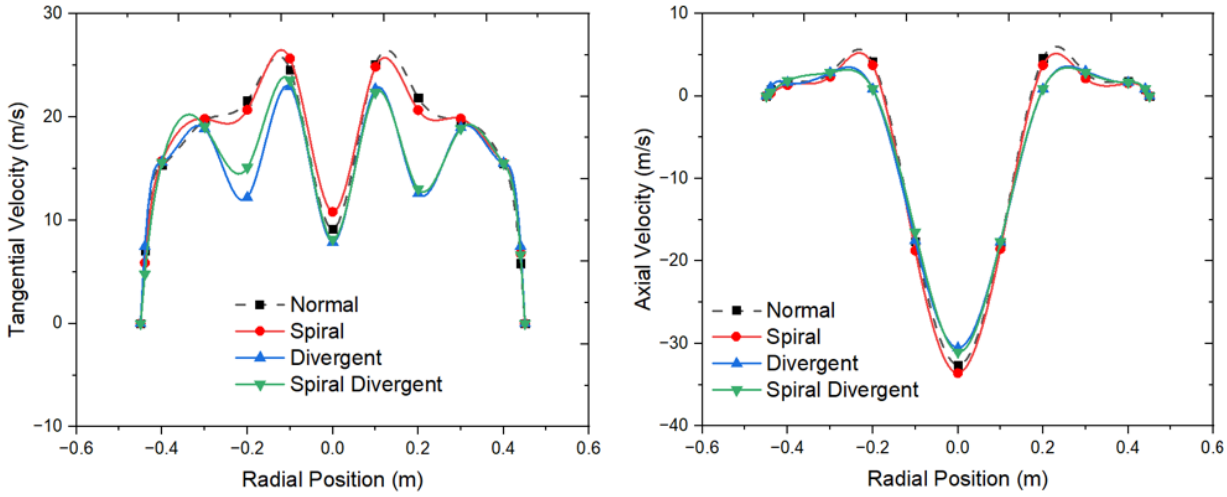

(a) (b)

Fig. 8. Tangential and axial velocity of different vortex finder shape at Z1 = 0.419m

The result from Figure 6(b), Figure 9 and Figure 10 reveals interesting insights into the relationship between vortex finder shape, particle track time, and particle separation efficiency in cyclone separators. Figure 11 and 12, shows the particle track time and path for 1 and 7 µm diameter particles. In Figure 11, it can be seen that for normal vortex finder's particle are escaping through short circuit flow near the opening of vortex finder. For other shapes, the escaping short circuit flow occur in the middle of the cyclone. In Figure 12, 7 µm particles seem to have chaotic movement in bin area of spiral vortex finder mostly, but the particle follows the swirling motion in normal vortex finder cyclone separator.

The particle resident time is also another important aspect to observe from these figures. Smaller particles as 1 µm seem to have less resident time than 7 µm particles. 1 µm particles take around maximum 6 to 8 seconds to be collected while 7 µm particles took around 14 to 17 seconds. The

reason behind the difference in gas time can be seen from the distinguished behavior of the particles 1 and 7 µm. 7 µm particles seen to stuck long time in swirling motion inside the cyclone due to centrifugal force effect the large particle in greater extent than smaller particles.

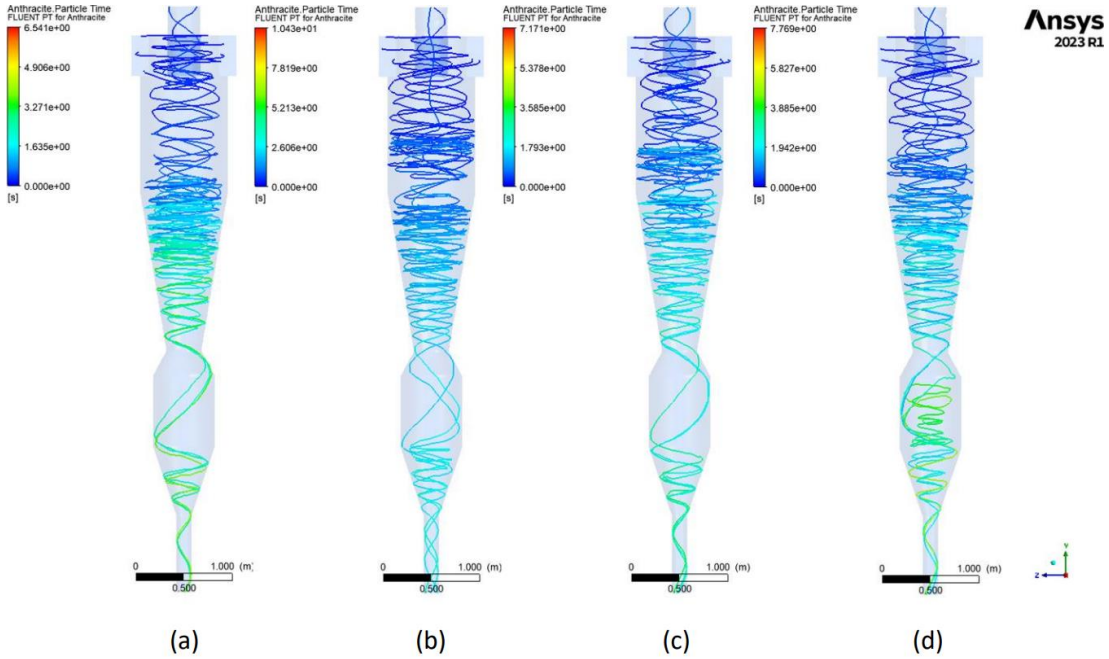

Fig. 9. 1µm Particle time for different vortex finder shape cyclone separator (a) Normal, (b) Spiral, (c) Divergent, and (d) Spiral Divergent

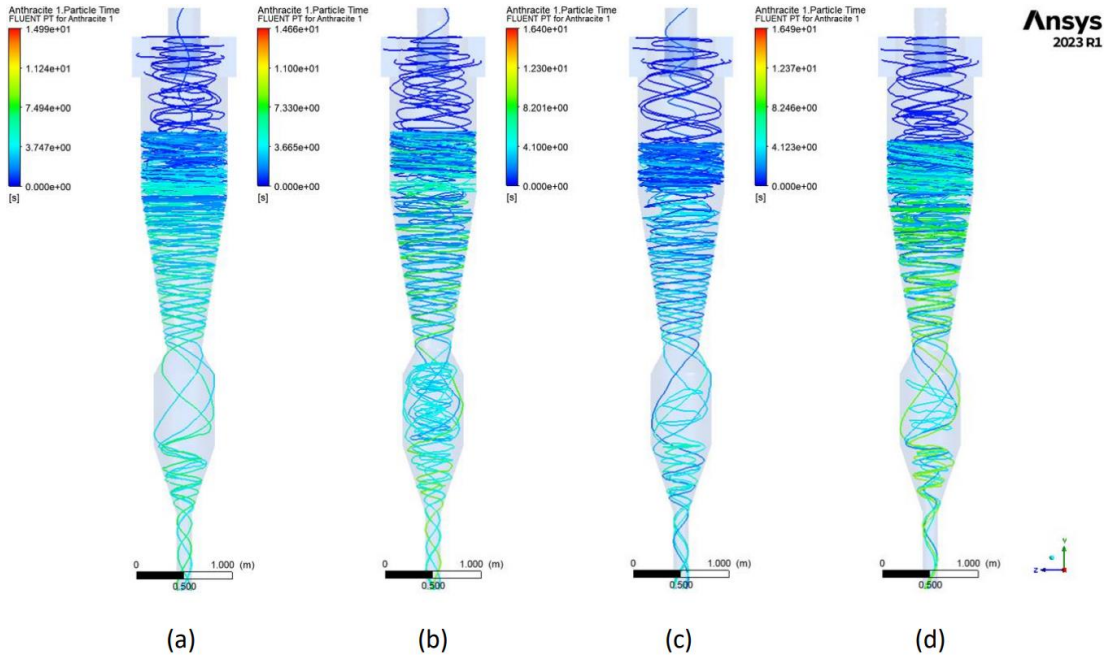

Fig. 10. 7µm Particle time for different vortex finder shape cyclone separator (a) Normal, (b) Spiral, (c) Divergent, and (d) Spiral Divergent

Figure 11 shows the velocity magnitude of normal, spiral, divergent and spiral divergent vortex finder. The velocity distribution of normal and spiral shape vortex finder is almost similar and highest magnitude occurred in the opening of vortex finder as upward gas stream narrowed to a smaller diameter. The sudden rise in gas velocity dropped in divergent shaped vortex finder as a result it gives a good distribution of velocity in all over the vortex finder. Combining the spiral and divergent elements into a spiral-divergent vortex finder, which is a novel design aimed at synergizing the benefits of both configurations. The velocity profile in this case reveals a complex pattern where the flow is forced to spiral while also diverging, potentially maximizing the efficiency of the cyclone separator.

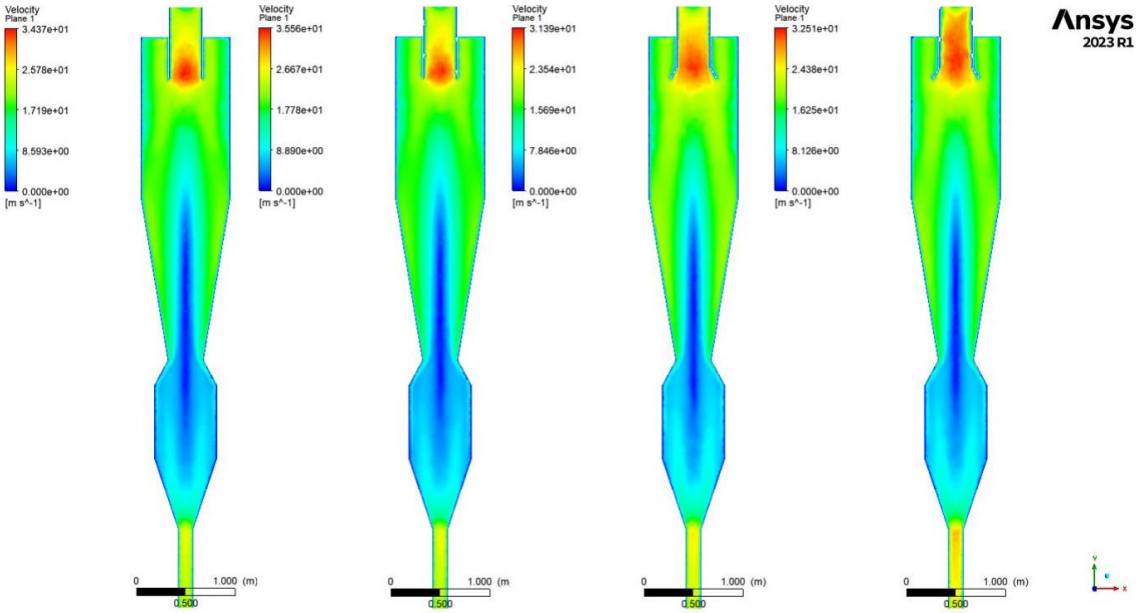

Fig.11. Velocity magnitude of different vortex finder shape (a) Normal, (b) Spiral, (c) Divergent, and (d) Spiral Divergent

The common between these different shapes is that the middle section or the inner vortex area have lower pressure compare to wall adjacent or outer vortex (Figure 12). Although, the normal and spiral vortex finder has a water drop shape of low-pressure region in the vortex finder. This shape takes a tubular form in the spiral-divergent vortex finder. The divergent shapes provide the room for uniform velocity distribution without creating sudden obstruction.

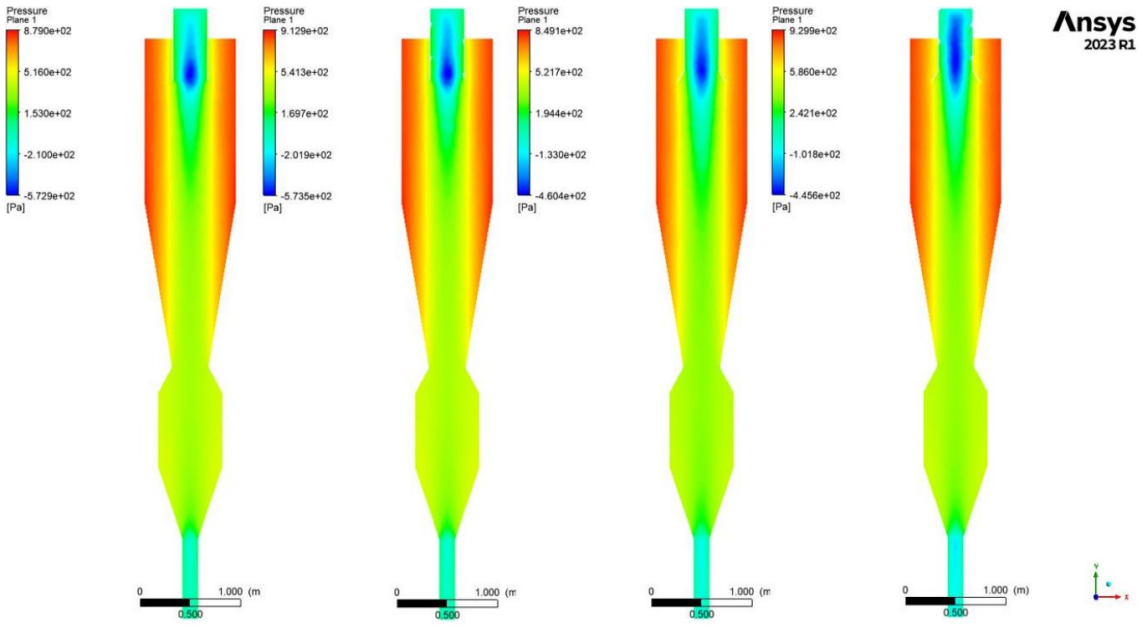

(a) (b) (c) (d)

Fig. 12. Total pressure of different vortex finder shape (a) Normal, (b) Spiral, (c) Divergent, and (d) Spiral Divergent

4. Conclusions

To study the performance of different shape and diameter of vortex finder CFD method has been used in this study. This study included five different vortex diameter sizes and four different vortex finder shapes. The performance was evaluated with pressure drop, collection efficiency, particle gas time, vorticity magnitude and total pressure. The results are concluded as follows

i. Among the five different vortex finder sizes, smallest diameters vortex finders prove to be best in terms of particle collection efficiency with high pressure drop. While, 366mm have the lowest particle collection efficiency and the pressure drop.
ii. Divergent vortex finder performance in terms of particle collection efficiency is highest and pressure drop is lowest among the other shapes. The result advises that vortex finder body should produce less friction and obstruction for a smooth flow.
iii. The relation between particle gas time and pressure drop prove to be directly proportional. On the contrary, the particle collection efficiency is inversely proportional to the particle gas time and pressure drop.

This study emphasizes the importance of vortex finder shape and dimeter for improved performance of cyclone separator. The particle track line, vorticity magnitude and total pressure shows that how the geometry of vortex finder could affect the gas flow and particle trajectory. The findings of this study, could help the further improvement of cyclone separator and their application across various industrial settings.

Acknowledgment
The authors express their gratitude to Universiti Tun Hussein Onn Malaysia (UTHM) for their unwavering support throughout the research project. The study was made possible through financial assistance from the Tier 1 Research Grant Scheme Vot Q144.

References

[1] Hoffmann, Alex C., Louis E. Stein, and P. Bradshaw. "Gas cyclones and swirl tubes: principles, design and operation." *Applied Mechanics Reviews* 56, no. 2 (2003): B28-B29. https://doi.org/10.1115/1.1553446

[2] Mobley, R. Keith. "Dust collection systems." *Plant Engineer's Handbook* (2001): 839-843. https://doi.org/10.1016/b978-075067328-0/50049-5

[3] Kitamura, Osamu, and Makoto Yamamoto. "Proposal of a Reynolds Stress Model for Gas-Particle Turbulent Flows and its Application to Cylone Separators." In *Engineering Turbulence Modelling and Experiments* 4, pp. 893-902. Elsevier Science Ltd, 1999. https://doi.org/10.1016/B978-008043328-8/50086-2

[4] Li, Wansong, Zhiqiang Huang, and Gang Li. "Improvement of the cyclone separator performance by the wedge-shaped roof: A multi-objective optimization study." *Chemical Engineering Science* 268 (2023): 118404. https://doi.org/10.1016/j.ces.2022.118404

[5] Brar, Lakhbir Singh, and Marek Wasilewski. "Investigating the effects of temperature on the performance of novel cyclone separators using large-eddy simulation." *Powder Technology* 416 (2023): 118213. https://doi.org/10.1016/j.powtec.2022.118213

[6] Pandey, Satyanand, and Lakhbir Singh Brar. "Performance analysis of cyclone separators with bulged conical segment using large-eddy simulation." *Powder Technology* 425 (2023): 118584. https://doi.org/10.1016/j.powtec.2023.118584

[7] Bumrungthaichaichan, Eakarach. "A note of caution on numerical scheme selection: Evidence from cyclone separator CFD simulations with appropriate near-wall grid sizes." *Powder Technology* 427 (2023): 118713. https://doi.org/10.1016/j.powtec.2023.118713

[8] Fatahian, Hossein, Esmaeel Fatahian, and Rasool Erfani. "Square cyclone separator: performance analysis optimization and operating condition variations using CFD-DPM and Taguchi method." *Powder Technology* 428 (2023): 118789. https://doi.org/10.1016/j.powtec.2023.118789

[9] Sardar, Rajdeep, Jinho Oh, Mirae Kim, Jung-Eon Lee, Seungho Kim, and Kyung Chun Kim. "The effect of inlet velocity, gas temperature and particle size on the performance of double cyclone separator." *Chemical Engineering and Processing-Process Intensification* 191 (2023): 109469. https://doi.org/10.1016/j.cep.2023.109469

[10] Chaghakaboodi, Hooman Abdi, and Maysam Saidi. "Numerical study of gas-solid flow in a square cyclone separator with different vortex finders." *Chemical Engineering Research and Design* 194 (2023): 621-635. https://doi.org/10.1016/j.cherd.2023.05.001

[11] Yang, Honggang, Nan Wang, Yingxue Cao, Xiaojing Meng, and Lei Yao. "Effects of helical fins on the performance of a cyclone separator: A numerical study." *Advanced Powder Technology* 34, no. 1 (2023): 103929. https://doi.org/10.1016/j.apt.2022.103929

[12] Gopalakrishnan, B., G. Saravana Kumar, and K. Arul Prakash. "Parametric analysis and optimization of gas-particle flow through axial cyclone separator: A numerical study." *Advanced Powder Technology* 34, no. 2 (2023): 103959. https://doi.org/10.1016/j.apt.2023.103959

[13] Guo, Ming, Yilin Lu, Chuanzhi Xue, Xun Sun, and Joon Yong Yoon. "The impact of cylinder vortex stabilizer on fluctuating turbulence characteristics of a cyclone separator based on Large Eddy Simulation." *Advanced Powder Technology* 34, no. 9 (2023): 104149. https://doi.org/10.1016/j.apt.2023.104149

[14] Yao, Yuge, Manxia Shang, Xiwei Ke, Zhong Huang, Tuo Zhou, and Junfu Lyu. "Effects of the inlet particle spatial distribution on the performance of a gas-solid cyclone separator." *Particuology* 85 (2024): 133-145. https://doi.org/10.1016/j.partic.2023.03.024

[15] Wang, Zetao, Guogang Sun, and Yunnan Jiao. "Experimental study of large-scale single and double inlet cyclone separators with two types of vortex finder." *Chemical Engineering and Processing-Process Intensification* 158 (2020): 108188. https://doi.org/10.1016/j.cep.2020.108188

[16] Barua, Saikat, Azriszul Mohd Amin, Akmal Nizam Mohammed, Mohd Faizal Mohideen Batcha, and Makatar Wae-hayee. "Experimental Study on the Relation between the Energy Efficiency and Pressure Drop of Dual Inlet Cyclone Separator in Processing Indoor Farming Biomass Waste." *Journal of Advanced Research in Applied Mechanics* 104, no. 1 (2023): 46-58. https://doi.org/10.37934/aram.104.1.4658

[17] Batcha, Mohd Faizal Mohideen, Muhammad Fazli Othaman, Sulastri Sabudin, Akmal Nizam Mohammed, Mohammad Kamil Abdullah, and Mas Fawzi Mohd Ali. "Combustion and emission of pelletized empty fruit bunch and oil palm shell in a swirling fluidized bed combustor." *Biomass Conversion and Biorefinery* 10 (2020): 755-763. https://doi.org/10.1007/s13399-020-00903-x

[18] Barua, Saikat, Azriszul Mohd Amin, Akmal Nizam Mohammed, Mohd Faizal Mohideen Batcha, and Makatar Wae-hayee. "A Comparative Study Between Turbulence Model RSM Results of a Dual Inlet Cyclone Separator and K-Epsilon RNG Turbulence Model." In *International Conference and Exhibition on Sustainable Energy and Advanced*

Materials, pp. 385-389. Singapore: Springer Nature Singapore, 2023. https://doi.org/10.1007/978-981-97-0106-3_61

[19] Elhashimi, Mohammed A., Michelle Gee, and Bahman Abbasi. "Unconventional desalination: The use of cyclone separators in HDH desalination to achieve zero liquid discharge." *Desalination* 539 (2022): 115932. https://doi.org/10.1016/j.desal.2022.115932

[20] Jola, Jola. "RNG k-epsilon model." *CFD Online*. June 11, 2007.